The Spectral Element method for three-dimensional seismic wave propagation

Dimitri Komatitsch[*] and Jeroen Tromp, EPS, Harvard University

Introduction

The accurate calculation of seismograms in realistic 3-D Earth models has become a necessity in seismology. A large arsenal of numerical techniques is available for this purpose. Among them, the most widely used approach is probably the finite-difference method (Virieux, 1986). Unfortunately, significant difficulties arise in the presence of surface topography and when anisotropy needs to be incorporated. Pseudospectral methods have become popular, but are restricted to models with smooth variations. The spectral-element method used here was introduced fifteen years ago in computational fluid dynamics (Patera, 1984). It has recently gained interest for problems related to 2-D (Seriani et al., 1992; Tordjman, 1995) and 3-D (Komatitsch and Vilotte, 1998; Faccioli et al., 1997; Komatitsch and Tromp, 1999) wave propagation. The method easily incorporates free surface topography and accurately represents the propagation of surface waves. The effects of anisotropy (Komatitsch et al., 2000a) and fluid-solid boundaries (Komatitsch et al., 2000b) can also be accommodated. The method lends itself well to parallel computation with distributed memory (Komatitsch and Vilotte, 1998).

Equations of Motion

The displacement field $\mathbf{s}$ produced by an earthquake is governed by the momentum equation $\rho \, \partial_t^2 \mathbf{s} = \boldsymbol{\nabla} \cdot \mathbf{T} + \mathbf{f}$. The distribution of density is denoted by ρ. The stress tensor $\mathbf{T}$ is linearly related to the displacement gradient $\boldsymbol{\nabla}\mathbf{s}$ by Hooke's law, which in an elastic, anisotropic solid may be written in the form $\mathbf{T} = \mathbf{c} : \boldsymbol{\nabla}\mathbf{s}$. In an attenuating medium, Hooke's law needs to be modified such that the stress is determined by the entire strain history:

$$\mathbf{T}(t) = \int_{-\infty}^{\infty} \partial_t \mathbf{c}(t - t') : \boldsymbol{\nabla}\mathbf{s}(t') \, \mathrm{d}t'. \qquad (1)$$

In seismology, the quality factor Q is observed to be constant over a wide range of frequencies. Such an *absorption-band solid* may be mimicked by a series of L standard linear solids, in the form

$$c_{ijkl}(t) = c_{ijkl}^{R}\left[1 - \sum_{\ell=1}^{L}(1 - \tau_{ijkl}^{\epsilon\ell}/\tau^{\sigma\ell})e^{-t/\tau^{\sigma\ell}}\right]H(t), \qquad (2)$$

where c_{ijkl}^{R} denotes the relaxed modulus, and $H(t)$ is the Heaviside function. Using the absorption-band anelastic

tensor (2), the constitutive relation (1) may be rewritten in the form $\mathbf{T} = \mathbf{c}^{U} : \boldsymbol{\nabla}\mathbf{s} - \sum_{\ell=1}^{L} \mathbf{R}^{\ell}$, where for each standard linear solid

$$\partial_t \mathbf{R}^{\ell} = -\mathbf{R}^{\ell}/\tau^{\sigma\ell} + \boldsymbol{\delta}\mathbf{c}^{\ell} : \boldsymbol{\nabla}\mathbf{s}/\tau^{\sigma\ell}. \qquad (3)$$

The components of the unrelaxed modulus c_{ijkl}^{U} are given by

$$c_{ijkl}^{U} = c_{ijkl}^{R}\left[1 - \sum_{\ell=1}^{L}(1 - \tau_{ijkl}^{\epsilon\ell}/\tau^{\sigma\ell})\right], \qquad (4)$$

and the modulus defect $\boldsymbol{\delta}\mathbf{c}^{\ell}$ associated with each individual standard linear solid is determined by

$$\delta c_{ijkl}^{\ell} = -c_{ijkl}^{R}(1 - \tau_{ijkl}^{\epsilon\ell}/\tau^{\sigma\ell}). \qquad (5)$$

We use the equivalent weak form of these equations

$$\int_{\Omega} \rho \, \mathbf{w} \cdot \partial_t^2 \mathbf{s} \, \mathrm{d}^3\mathbf{x} = -\int_{\Omega} \boldsymbol{\nabla}\mathbf{w} : \mathbf{T} \, \mathrm{d}^3\mathbf{x} \qquad (6)$$

where the stress tensor $\mathbf{T}$ is determined in terms of the displacement gradient $\boldsymbol{\nabla}\mathbf{s}$ by Hooke's law.

Elements

Each hexahedral spectral element Ω_e can be mapped to a reference cube. Points within this reference cube are denoted by $\boldsymbol{\xi} = (\xi, \eta, \zeta)$. At least eight corner nodes are needed to define a hexahedral volume element; by adding mid-side and center nodes the number of anchors can become as large as 27.

Integrations over the volume Ω are subdivided into smaller integrals over the volume elements Ω_e. The control points ξ_{α}, $\alpha = 0, \ldots, n_{\ell}$, needed in the definition of the Lagrange interpolation polynomials of degree n_{ℓ} are chosen to be the $n_{\ell} + 1$ Gauss-Lobatto-Legendre points. These points can be computed numerically.

In a SEM for wave propagation problems one typically uses a polynomial degree n_{ℓ} between 5 and 10 to represent a function on the element (Komatitsch and Vilotte, 1998). On each volume element Ω_e a function f is interpolated by triple products of Lagrange polynomials of degree n_{ℓ} as:

$$f(\mathbf{x}(\xi, \eta, \zeta)) \approx \sum_{\alpha,\beta,\gamma=0}^{n_{\ell}} f^{\alpha\beta\gamma}\ell_{\alpha}(\xi)\ell_{\beta}(\eta)\ell_{\gamma}(\zeta), \qquad (7)$$

where $f^{\alpha\beta\gamma} = f(\mathbf{x}(\xi_{\alpha}, \eta_{\beta}, \zeta_{\gamma}))$. Using this polynomial representation, the gradient of a function, $\boldsymbol{\nabla}f$, may be written in the form

$$\boldsymbol{\nabla}f(\mathbf{x}(\xi, \eta, \zeta)) \approx \sum_{i=1}^{3} \hat{\mathbf{x}}_i \partial_i f(\mathbf{x}(\xi, \eta, \zeta)) \qquad (8)$$

where differentiation in the reference domain is performed by analytically differentiating the Lagrange interpolation polynomials.

At this stage, integrations over element Ω_e may be approximated using the Gauss-Lobatto-Legendre integration rule

$$\int_{\Omega_e} f(\mathbf{x})\, \mathrm{d}^3\mathbf{x} = \int\int\int f(\mathbf{x}(\xi,\eta,\zeta))\, J_e(\xi,\eta,\zeta)\, \mathrm{d}\xi\, \mathrm{d}\eta\, \mathrm{d}\zeta$$

$$\approx \sum_{\alpha,\beta,\gamma=0}^{n_\ell} \omega_\alpha \omega_\beta \omega_\gamma f^{\alpha\beta\gamma} J_e^{\alpha\beta\gamma}. \quad (9)$$

To facilitate the integration of functions and their partial derivatives over the elements, the values of the inverse Jacobian matrix $\partial\boldsymbol{\xi}/\partial\mathbf{x}$ need to be stored at the $(n_\ell + 1)^3$ Gauss-Lobatto-Legendre integration points for each element.

Global system and time marching

Before the system can be marched forward in time, the contributions from all the elements that share a common global grid point need to be summed. In a traditional FEM this is referred to as the *assembly* of the system. Let U denote the displacement vector of the global system. The ordinary differential equation that governs the time dependence of the global system may be written in the form $M\ddot{U} + C\dot{U} + KU = F$, where M denotes the global mass matrix, C the global absorbing boundary matrix, K the global stiffness matrix, and F the source term. Further details on the construction of the global mass and stiffness matrices can be found in (Komatitsch and Vilotte, 1998). A highly desirable property of a SEM, which allows for a very significant reduction in the complexity and cost of the algorithm, is the fact that the mass matrix M is diagonal by construction. Therefore, no costly linear system resolution algorithm is needed to march the system in time (Komatitsch and Vilotte, 1998; Komatitsch and Tromp, 1999). Time discretization of the second-order ordinary differential equation is achieved based upon a classical explicit second-order finite-difference scheme. Such a scheme is conditionally stable, and the Courant stability condition is governed by the minimum value of the ratio between the size of the grid cells and the P-wave velocity.

Numerical results: layer-cake models

We study a simple but difficult model consisting of a layer over a half-space, as shown in Figure 1. The horizontal size of the block used is 134 km × 134 km, and the block extends to a depth of 60 km. The non-structured mesh shown in Figure 2 is composed of 68208 elements, using a polynomial degree $N = 5$, which results in 8743801 points. The source is a vertical force located in the middle of the grid at a depth of 25.05 km. The solution includes strong multiples in addition to the direct P and
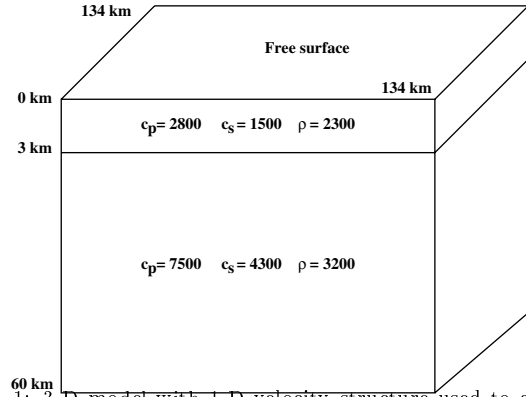
Fig. 1: 3-D model with 1-D velocity structure used to assess the efficiency of the non-structured brick of Figure 2. We study a model consisting of a layer over a half-space. The horizontal size of the block is 134 km × 134 km, and it extends to a depth of 60 km.
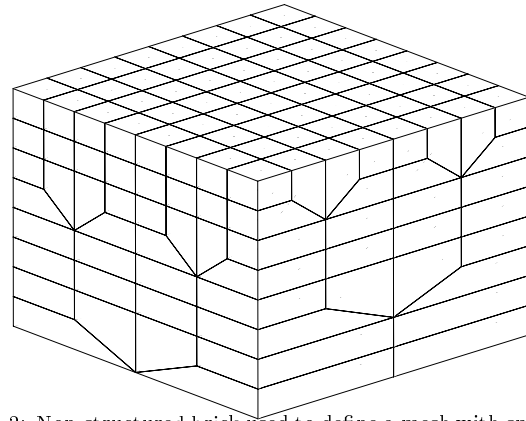
Fig. 2: Non-structured brick used to define a mesh with smaller elements at the top of the structure. We apply a geometrical grid doubling in the horizontal directions.

S waves. The source is a Ricker wavelet with a maximum frequency of 1 Hz. The time step is $\Delta t = 6.5$ ms, and we propagate the signal for 40 s. A line of receivers is placed at the surface along the y-axis at $x = x_{\max}/2 = 67$ km.

Traces recorded at a receiver at a horizontal distance of 31.11 km from the source are shown in Figure 3 for two of the components of the displacement vector, the third (tangential) component being zero by symmetry. The strong direct P and S waves can be clearly observed, as well as strong multiples generated by the layer. We compare the SEM results to those based upon a discrete-wavenumber/reflectivity method. The agreement is very good. Small parasitic phases reflected from the absorbing boundaries explain the small discrepancies observed between $t = 30$ and $t = 35$ s. We implemented the parallel algorithm based upon the Message-Passing Interface (MPI) on distributed-memory machines. The total CPU time on a 8-node Dec Alpha was roughly 8 hours. We obtained a total sustained performance of 1.3 Gigaflop, a parallel speedup of 7.3, and a parallel efficiency of 91 %. The total memory needed was roughly 1 Gigabyte. The

Spectral Elements for 3D seismic wave propagation

MPI code was also successfully run on a network of PCs under Linux (Beowulf).
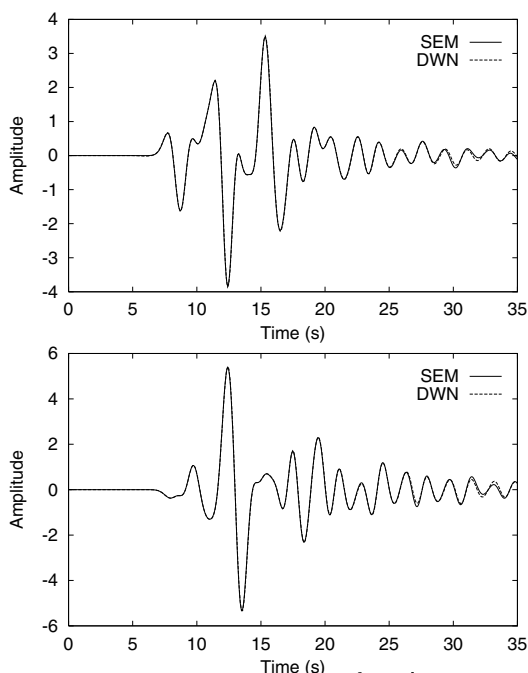
Fig. 3: Traces recorded at the surface for a layer over a half-space. The source is located at a depth of 25.05 km. The receiver is located at a horizontal distance of 31.11 km. The vertical (top) and radial (bottom) components of displacement are compared to the discrete-wavenumber reference. Numerous strong multiples are clearly visible.

Hemispherical crater

(Sánchez-Sesma, 1983) studied the response of a hemispherical crater in a homogeneous half-space to a vertically incident plane P-wave based upon an approximate boundary method. He presented the displacement recorded at the surface for different normalized frequencies $\eta = 2a/\lambda_P$, where a is the radius and λ_P the wavelength of the incident P-wave. We compute the amplitude of the displacement at the surface along a profile for two values of the normalized frequency, $\eta = 0.25$ and $\eta = 0.50$, as a function of the normalized horizontal coordinate x/a between 0 and 2. Poisson's ratio is equal to 0.25.

The mesh is composed of 1800 elements, with a polynomial degree $N = 4$ in each element; the global mesh contains 120089 points. Considering a P-wave velocity of $c_p = 1732$ m.s^{-1} and an S-wave velocity of $c_s = 1000$ m.s^{-1}, the time step used is $\Delta t = 5$ ms, and the signal is propagated for 16 s. The density is 1000 kg.m^{-3}. The source is a Ricker wavelet with dominant frequency $f_0 = \sqrt{3}/4$ Hz. Figure 4 shows a comparison in the frequency domain for $\eta = 0.25$ and $\eta = 0.50$. The agreement is excellent. The strong amplification close to the edges is well reproduced. The amplification level of the vertical
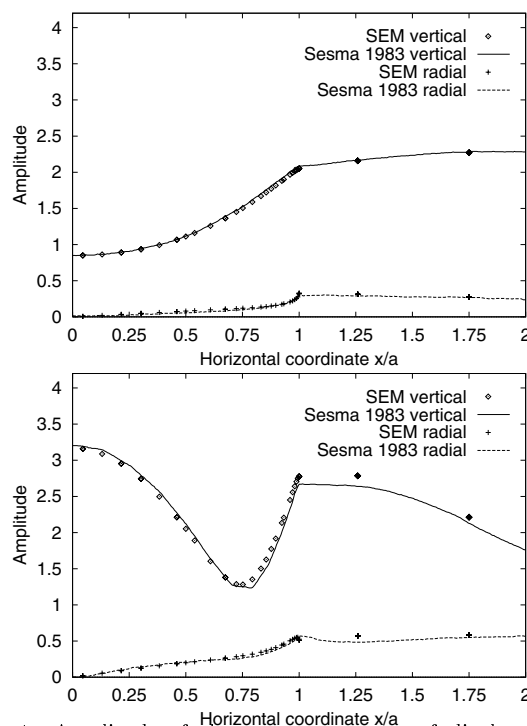
Fig. 4: Amplitude of the two components of displacement recorded along the crater, from the center to $x/a = 2$ km. The vertical and radial components are displayed. The third (tangential) component is zero by symmetry. The results are shown for two normalized frequencies, $\eta = 0.25$ (top) and $\eta = 0.50$ (bottom). The solid and dashed lines are the results of Sánchez-Sesma (1983).

component reaches a very high value ($\simeq 3.2$) in the center for $\eta = 0.50$.

Homogeneous model with strong attenuation

We consider a 2-D homogeneous medium of size 2000 m × 2000 m. Strong attenuation represented by constant $Q_P \simeq 30$ and $Q_S \simeq 20$ is introduced. The relaxed (elastic) velocities of the medium are $c_p = 3000$ m.s^{-1} and $c_s = 2000$ m.s^{-1}. The density is 2000 kg.m^{-3}. We expect very significant physical velocity dispersion. The source is a vertical force in the middle of the model. Its time variation is a Ricker wavelet with dominant frequency $f_0 = 18$ Hz. The constant values $Q_P \simeq 30$ and $Q_S \simeq 20$ are mimicked using two standard linear solids as in (Carcione et al., 1988).

The medium is discretized using 44 × 44 spectral elements, with a polynomial degree $N = 5$. The global grid comprises 221 × 221 = 48841 points. We use a fourth-order Runge-Kutta scheme to march the strong form of the memory variable equations. The time step is $\Delta t = 0.75$ ms. We propagate the signal for 0.75 s. In Figure 5 we present both the SEM and the analytical solutions for a receiver located at $x_r = z_r = 1500$ m. The agreement is very good. The amplitude of the S-wave is
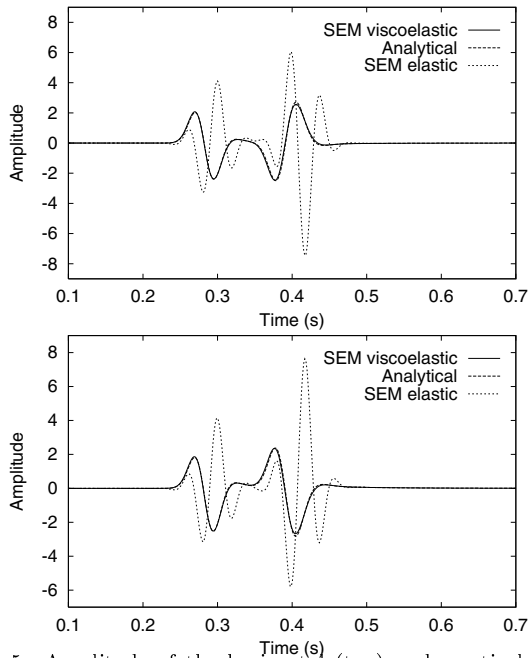
Fig. 5: Amplitude of the horizontal (top) and vertical (bottom) component of displacement recorded in a 2-D homogeneous medium with constant $Q_P \simeq 30$ and $Q_S \simeq 20$. We present both the spectral-element solution (solid line) and the analytical solution of Carcione et al. (1988) (dashed line). The very strong effect of attenuation can be observed by comparison with an elastic medium with the same relaxed material properties (dotted line).

reduced by a factor of more than two with respect to a purely elastic simulation.

Conclusions

We have presented a spectral-element method for 3-D seismic wave propagation. It incorporates surface topography, attenuation and anisotropy, and accurately represents surface waves. We have benchmarked the method against a discrete-wavenumber/reflectivity method for a layer-cake model. The accuracy of the free-surface implementation was demonstrated for a hemispherical crater embedded in a homogeneous half-space. The effects of attenuation were incorporated based upon an absorption-band model, and validated by comparison with the analytical solution.

References

Carcione, J. M., Kosloff, D., and Kosloff, R., 1988, Wave propagation simulation in a linear viscoelastic medium: Geophys. J. Int., **95**, 597–611.

Faccioli, E., Maggio, F., Paolucci, R., and Quarteroni, A., 1997, 2D and 3D elastic wave propagation by a pseudo-spectral domain decomposition method: J. Seismol., **1**, 237–251.

Komatitsch, D., and Tromp, J., 1999, Introduction to the spectral-element method for 3-D seismic wave propagation: Geophys. J. Int., **139**, 806–822.

Komatitsch, D., and Vilotte, J. P., 1998, The Spectral Element method: an efficient tool to simulate the seismic response of 2D and 3D geological structures: Bull. Seis. Soc. Am., **88**, no. 2, 368–392.

Komatitsch, D., Barnes, C., and Tromp, J., 2000a, Simulation of anisotropic wave propagation based upon a spectral element method: Geophysics.

———— 2000b, Wave propagation near a fluid-solid interface: a spectral element approach: Geophysics, **65**, no. 2.

Patera, A. T., 1984, A spectral element method for fluid dynamics: laminar flow in a channel expansion: J. Comput. Phys., **54**, 468–488.

Sánchez-Sesma, F. J., 1983, Diffraction of elastic waves by three-dimensional surface irregularities: Bull. Seis. Soc. Am., **73**, no. 6, 1621–1636.

Seriani, G., Priolo, E., Carcione, J. M., and Padovani, E., 1992, High-order spectral element method for elastic wave modeling: Expanded abstracts of the Soc. Expl. Geophys., 1285–1288.

Tordjman, N., 1995, Éléments finis d'ordre élevé avec condensation de masse pour l'équation des ondes: Ph.D. thesis, Université Paris IX Dauphine, Paris, France.

Virieux, J., 1986, P-SV wave propagation in heterogeneous media: velocity-stress finite-difference method: Geophysics, **51**, 889–901.